JOURNAL OF AIRCRAFT
Vol. 46, No. 1, January–February 2009

Advanced Design by Numerical Methods and Wind-Tunnel Verification Within European High-Lift Program

Jochen Wild* and Joel Brezillon†
DLR, German Aerospace Center, 38162 Brunswick, Germany
Olivier Amoignon‡
Swedish Defence Research Agency, 164 90 Stockholm, Sweden
Jürgen Quest§
European Transonic Wind Tunnel, GmbH, 51147 Cologne, Germany
Frederic Moens¶
ONERA, 92322 Châtillon, France
and
Domenico Quagliarella**
Centro Italiano Ricerche Aerospaziali, 81043 Capua, Italy

DOI: 10.2514/1.37148

The design activity within the European sixth framework European High-Lift Program II is targeted toward an improvement of the takeoff performance of a generic transport aircraft configuration by a redesign of the trailing-edge flap. The involved partners applied different optimization strategies, as well as different types of flow solvers, to cover a wide range of possible approaches for aerodynamic design optimization. The optimization results obtained by the different partners have been cross calculated to eliminate solver dependencies and to identify the best obtained design. The final selected design has been applied to the wind-tunnel model, and the test in the European Transonic Wind Tunnel at high Reynolds number confirms the predicted improvements.

Nomenclature

C_D	=	drag coefficient
C_L	=	lift coefficient
$C_{L,\max}$	=	maximum lift coefficient
c	=	local wing chord
c_p	=	local pressure coefficient
D	=	drag force
F_i	=	objective function of design point i
F_{obj}	=	objective function
G	=	weight force
L	=	lift force
M	=	Mach number
P	=	penalty function
p	=	static pressure
p_t	=	stagnation pressure
$Sr\ Re$	=	Reynolds number
T	=	thrust
T_t	=	stagnation temperature
V_S	=	stall speed
w_i	=	weighting factor for the ith design point
$\mathbf{x}$	=	vector of design parameters
x, y, z	=	Cartesian coordinates (2-D: x chord, y up; 3-D: x chord, y span, z up)
x_F, y_F	=	flap positioning parameters
α	=	angle of attack
γ	=	glide or climb path angle
$\gamma_{C_L}, \gamma_{C_D}$	=	correlated scaling factors for aerodynamic force coefficients
η	=	dimensionless wingspan $\eta = 2y/b$
Λ	=	wing aspect ratio
$\tilde{\Lambda}$	=	transformed wing aspect ratio
φ	=	wing sweep angle

Subscripts

ini	=	initial calculation
2-D	=	two-dimensional flow (leading-edge normalization)
2.5-D	=	infinite swept wing flow
3-D	=	three-dimensional flow
∞	=	flow conditions at infinity

Presented as Paper 4300 at the 25th Applied Aerodynamics Conference, Miami, FL, 25–28 June 2007; received 14 February 2008; accepted for publication 21 July 2008.

*Research Scientist, Institute of Aerodynamics and Flow Technology, Transport Aircraft Department.
†Research Scientist, Institute of Aerodynamics and Flow Technology, Numerical Methods Department.
‡Research Engineer, Computational Physics Department.
§Chief Aerodynamicist, Senior AIAA Member.
¶Research Engineer, Applied Aerodynamics Department.
**Research Engineer, Applied Aerodynamics Laboratory.

I. Introduction

THE European High-Lift Program (EUROLIFT II) project, funded by the European Commission within the sixth framework program, is dedicated to the investigation of transport aircraft in high-lift configuration. It covers both numerical and experimental studies, mainly targeted toward validation of computational fluid dynamics (CFD) for maximum lift prediction of such configurations. It is a follow up to the EUROLIFT project of the fifth framework program [1]. Whereas, in the former project, a simplified wing–body high-lift configuration was investigated, the new project focuses on a more realistic configuration including engine nacelles, pylons, tracks, and brackets. Additionally, the next step is undertaken coming from analysis to design. Because it is a main aim of the project to deal with realistic configurations, this design will be done at a Reynolds number comparable to flight conditions of a real transport aircraft.

The design activity within the project is targeted toward an improvement of the aerodynamic properties of the KH3Y

wind-tunnel model configuration, which has already been used in EUROLIFT. The investigations mainly focus on an increased takeoff performance by modifying the trailing-edge flap both in shape and position. The design is mainly performed using numerical optimization methods for optimization of a specific wing section. The involved partners apply different optimization strategies, as well as different types of flow solvers to cover a wide range of possible approaches for aerodynamic design optimization. The flow calculation methods range from an Euler–boundary-layer code to structured and unstructured Reynolds-averaged Navier–Stokes (RANS) solvers, either in 2-D or 2.5-D. For optimization, a lot of different strategies are used, including gradient-based methods, simplex strategies, simulated annealing, evolutionary algorithms, and, last but not least, an industrial best practice approach.

The design activity is split up into three phases related to verification, design, and validation. At the beginning, a verification phase is scheduled, where a mandatory test case has been defined and optimized applying the available design strategies to assess the reliability and limitations of the design process. In the next phase, the design specification has been formulated, taking into the account the results of the verification phase. This case is now optimized by the different partners by using their numerical optimization processes. Afterward, the different optimization results are cross checked to identify the best obtained design. In the validation phase of the project, the best design is applied to the three-dimensional wind-tunnel model and is measured in the European Transonic Wind Tunnel (ETW) at high Reynolds numbers close to real flight conditions.

The work share between the partners within the design task was constructed to assess as many different strategies as possible. For this reason, the different partners apply different optimization strategies as well as different levels of flow simulation accuracy. The optimization strategies applied include gradient-based methods, simplex strategies, and evolutionary algorithms. For the flow calculations, Euler–boundary-layer coupling methods (Euler-BL), RANS methods, and additionally parabolized stability equation methods for transition prediction are used.

II. Mandatory Test Case Calculations

The aim of this activity was to demonstrate the optimization capabilities by each partner and to ensure that the tools are available and applicable for the further work of this work package.

A. Optimization Case Definition

The selected design case was extracted from wind-tunnel data obtained in the EUROLIFT I project, so that a correlation of numerically detected optimum and experimental data has been possible. The optimization problem considered here is a multipoint design for the wing section of a landing configuration. Three main objectives are active when dealing with a landing configuration: 1) high maximum lift coefficients for low approach speeds and/or high aircraft capacity, 2) attached flow in the complete flight regime, and 3) high L/D at $1.13V_S$, because the landing configuration may be used for noise classification, where overflow heights at the microphone location are maximal.

These objectives are translated into an objective function by

$$
\begin{aligned}
F_{\text{obj}}(\mathbf{x}) &= \sum_{i=1}^{3} w_i \cdot F_i(\mathbf{x}) \\
F_1(\mathbf{x}) &= -C_{L,\max} \\
F_2(\mathbf{x}) &= -C_L|_{\alpha=0\,\text{deg}} \\
F_3(\mathbf{x}) &= -\frac{C_L}{C_D + (C_L^2/\pi\Lambda)}, \quad C_L = C_{L,\max}/1.13^2, \quad \Lambda = 9.353
\end{aligned}
\tag{1}
$$

with $\mathbf{x}^T = (\Delta x_F, \Delta y_F)$, and $w_1 = 0.6$, $w_2 = 0.3$, and $w_3 = 0.1$. The three design points are defined as follows:

1) $M_\infty = 0.15$, $Re_\infty = 0.7 \times 10^6$, $\alpha =$ free.
2) $M_\infty = 0.22$, $Re_\infty = 1 \times 10^6$, $\alpha = 0$ deg.
3) $M_\infty = 0.17$, $Re_\infty = 0.8 \times 10^6$, $\alpha = f(C_L)$.

Two constraints should be applied: 1) $C_{L,\max} \geq C_{L,\max,\text{ini}}$ for the first design point, and 2) $C_L = C_{L,\text{target}} \pm 0.001$ for the third design point.

The geometry used is the wing section of the KH3Y model of EUROLIFT I in landing configuration (TC214) at the location of the pressure row named DV06 at the nondimensional span of $\eta = 0.66$ (Fig. 1). For further identification, this test case is named TC301.

B. Applied Methods

The applied methods for CFD simulation and numerical optimization cover the complete range of state of the art for aerodynamic simulation and design. Gradient-based, gradient-free, and stochastic optimization algorithms are incorporated. For CFD calculations, most of the partners applied finite volume methods based on the RANS equations. The equations are solved by a time-integration scheme. One partner applied an Euler-BL coupling method within the optimization loop.

Table 1 briefly summarizes the methods used by the involved partners. Airbus Germany (AD) used the unstructured RANS flow solver TAU, developed by DLR [2], in conjunction with an in-house unstructured mesh generator for 2-D unstructured meshes. Centro Italiano Ricerche Aerospaziali (CIRA) applied the well-known Euler–boundary-layer coupling flow solver MSES [3] in free transition mode. DLR used its in-house developed FLOWer code [4], which is a structured finite volume RANS solver. From several algebraic and transport turbulence equation models, the Spalart–Allmaras model with Edwards modification has been preferred for its accuracy and robustness. It was decided to generate new meshes at each optimization step, applying the parametric grid generator MegaCads [5] developed at DLR. All meshes are based on the same topology: a multiblock-type mesh with nine blocks; 90,065 points; and designed for three levels of multigrid. The Swedish Defence Research Agency (FOI) applied their flow solver EDGE [6], which solves the RANS equations on unstructured grids. The Spalart–Allmaras one-equation turbulence model is used here. Convergence is accelerated by local time stepping, multigrid, and implicit residual smoothing. Additionally, to account for natural transition, a linear stability analysis is applied [7]. ONERA used the ONERA elsA software [8] for the calculation of the aerodynamic coefficients, which solves the compressible three-dimensional RANS equations by using a cell-centered finite volume spatial discretization on structured multiblock meshes. Computations have been carried out

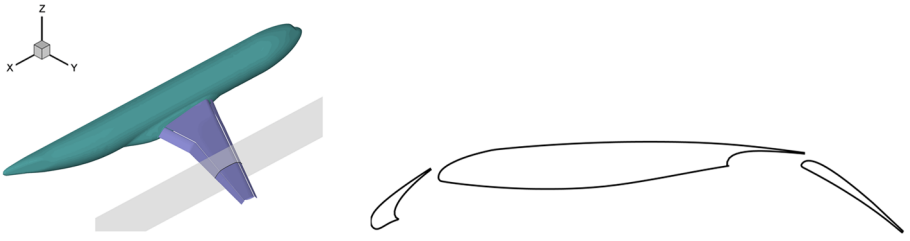

Fig. 1 Wing section of the KH3Y model in landing configuration at the location of pressure row DV06.

Table 1 Methods applied by the partners for the mandatory test case

Partner	Solver type	Grid type	Optimization algorithm
AD	RANS	Unstructured	Simulated annealing
CIRA	Euler-BL	Structured	Genetic algorithm
DLR	RANS	Structured	Simplex algorithm
FOI	RANS	Unstructured	Quasi-Newton method
ONERA	RANS	Structured	Conjugate gradient

using an uncoupled approach between the RANS system and the turbulence model transport equations. The two-equation k-ω model from Wilcox [9] with a wall function formulation [10] has been selected for the optimization work. This allows y^+ values around 100 and more regular cells, because such modifications increase robustness and make high Reynolds number computations less mesh dependent. During the EUROLIFT I program, comparison between classical structured multiblock and unstructured and structured chimera grids on the same configuration did not show dramatic differences [11].

For the optimization, all classes of strategies that exist today have been applied, including gradient-based, gradient-free, and stochastic methods. CIRA used a multi-objective genetic algorithm [12,13] for the optimization, with a crossover rate of 100%, a mutation rate of 1.5%, and local random walk as selection method for choosing the mating parents. Airbus Germany applied a simulating annealing algorithm embedded into the PointerPro optimization framework provided by Synaps [14]. This tool allows for an easy definition of design parameters, and fuzzy logic can be used for target function definition. The user can take advantage of task wizards and visual programming tools. DLR used a well-elaborated simplex method for this case, due to the very limited number of design variables [15]. It is a subspace-searching simplex method for the unconstrained optimization of general multivariate functions that generalizes the Nelder–Mead simplex method. This method is well suited for optimizing noisy functions, and, typically, the number of required function evaluations increases only with the problem size. FOI used a quasi-Newton method (Broyden–Fletcher–Goldfarb–Shanno update) to calculate descent directions in combination with a line search algorithm using Goldstein conditions [16]. The gradient of the objective function is estimated by a finite difference approximation, requiring, in the present case, 12 CFD solutions for one gradient. ONERA applied the conjugate gradient method CONMIN of Vanderplaats [17]. In the present methodology, the gradients are determined by finite differences at each iteration. For the accounting of the constraints, the feasible direction method of Zoutendijk is applied. The conjugation of the gradient is done according to Fletcher and Reeves. At each optimization iteration, three steps are performed to search for the objective function minimum along the search direction and to respect the constraints. The process for gradient computation has been parallelized, which means that, in terms of restitution time, the time requested of one optimization process is nearly equivalent to the number of iterations times the time needed for the flow solution.

Because of limitations of the applied CFD methods, some partners had to modify the design case to be able to compute. The main limitation herewith had been the missing functionality of automatic determination of the maximum lift coefficient. This functionality is included only into the flow solver of DLR. Airbus Germany uses an external process chain for this purpose that determines maximum lift coefficient by a sequence of flow calculations, while varying the angle of attack. CIRA and ONERA tackled this by using the angle of attack for the first design point as a design variable, which should lead to the maximum obtainable lift for the finally optimized configuration, but not for the initial one. FOI used a sequence of four CFD calculations and an L5-norm to estimate the maximum lift coefficient.

Additional adaptations to the design problem have been made by 1) CIRA, to compute the second design point at $\alpha = 2$ deg due to convergence problems at $\alpha = 0$ deg; 2) FOI, to not use second design point in the optimization due to convergence problems, and to omit the third design point in gradient computation; and 3) ONERA, to calculate the third design point at a constant angle of attack ($\alpha = 10$ deg), instead of a target lift computation.

C. Results

All partners delivered their optimization results, including 1) aerodynamic coefficients, surface pressure distributions, and flowfields of the initial and optimized configuration; 2) history of optimization in terms of design variables, aerodynamic coefficients, single objectives, and global objective; and 3) optimization statistics in terms of number of needed CFD calculations, CPU time, and turnaround (wall clock) time.

Figure 2 shows the results of the flap position optimizations for each partner. It is obvious that the bandwidth of the results is very large. Only the results of FOI and ONERA are close to each other. These results show a slight increase in flap gap, whereas all others show a gap reduction. The vertical displacement of the AD and DLR result are nearly identical, but the AD result is located more downstream. The result of CIRA is the one that is the most off from the others.

A detailed comparison of the provided data already showed that the calculations of the initial configuration show big differences among the partners. Figure 3 shows the pressure distributions for the initial configuration for each of the three design points. A similar spreading is observed for the optimized configurations (Fig. 4). Comparing each of the partners' results separately shows that the predicted improvements are reasonable related to the physics indicated by the flowfield of the baseline configuration. Very significant for the optimization results using the RANS methods is the detection of a flap separation for the initial configuration (AD, DLR) or attached flap flow (FOI, ONERA). Because of this flow feature, the flap gap is reduced for the first to eliminate the flap separation, whereas the gap is increased for the second to further increase maximum lift. The CIRA results are mainly identified to be dependent on the calculation method (Euler-BL), which is known to poorly simulate the flap boundary-layer interaction with the wake. Additional investigations by CIRA with their in-house RANS CFD-code verified the misleading sensitivity of the Euler-BL calculations for this type of flowfield.

D. Lessons Learned

From the results obtained from this mandatory design task, the main conclusions drawn are as follows:

1) All partners have their optimization environments running.

2) Different optimization results are related to differences in the flow for the initial configuration.

3) Better definition of initial configuration is needed.

4) Use of $C_{L,\max}$ in optimization is difficult to compare (only two partners have the possibility to directly detect $C_{L,\max}$, others use α as a design variable).

5) Detection of flap separation is critical and strongly solver dependent.

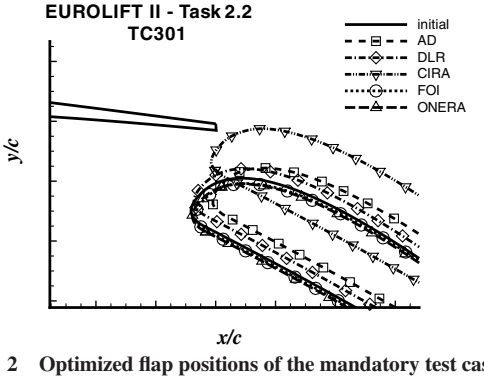

Fig. 2 Optimized flap positions of the mandatory test case.

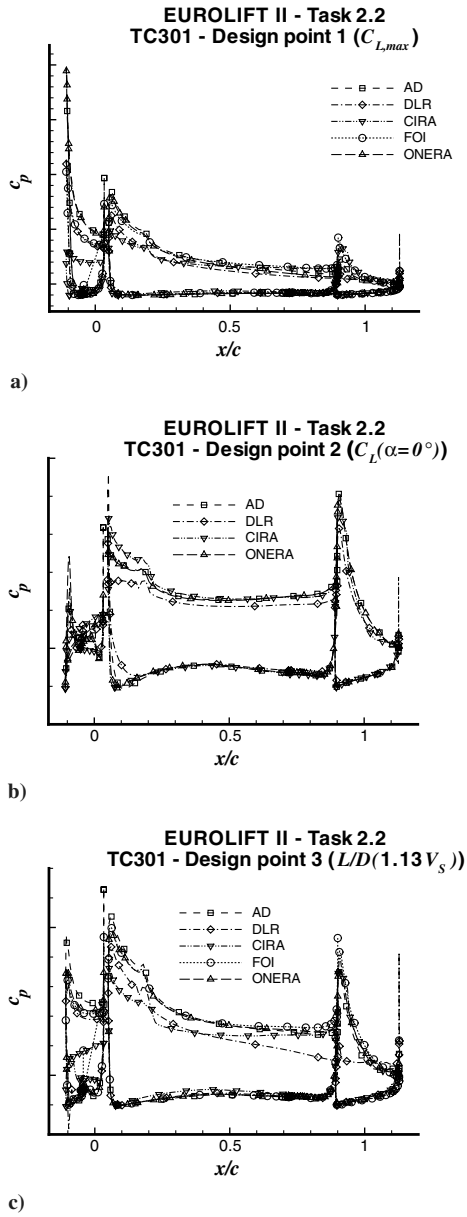

Fig. 3 Comparison of the pressure distributions of the initial configuration calculated by the different partners: a) maximum lift, b) lift in linear range, and c) lift-to-drag ratio for go-around.

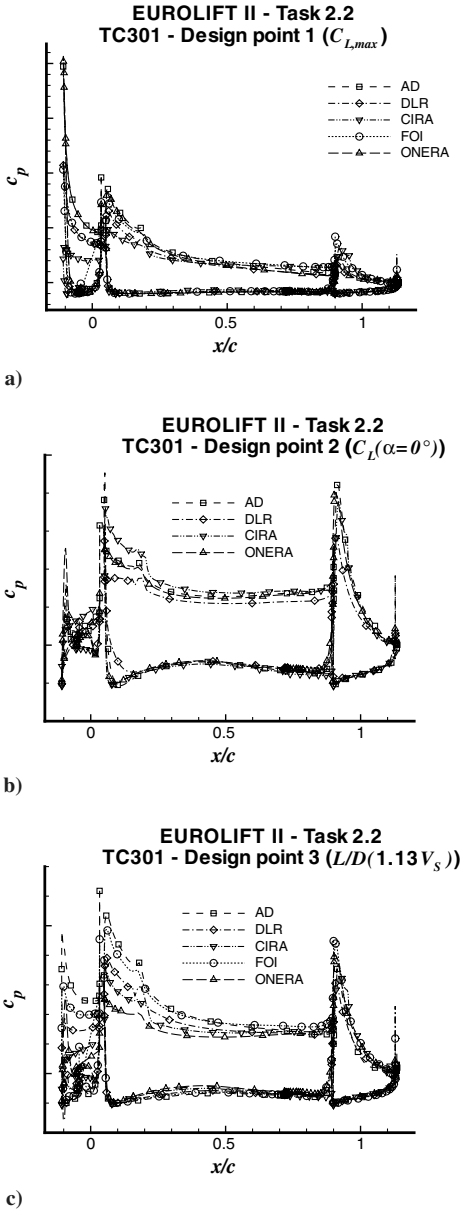

Fig. 4 Comparison of the pressure distributions of the optimum configuration calculated by the different partners: a) maximum lift, b) lift in linear range, and c) lift-to-drag ratio for go-around.

6) Evaluate usability of Euler-BL solver on initial configuration in comparison with RANS method depending on the properties of the flow.

These conclusions directed the following guidelines for the definition of the flap design specification:

1) Clearly define the initial configuration in more detail than with flow conditions only.

2) Do not use $C_{L,\max}$ directly for optimization, because capabilities are not commonly available.

3) Avoid flowfields with the chance of massive flap separation because of strong solver dependencies.

III. KH3Y Flap Design Optimization

The aim of this activity was to apply the numerical optimization capabilities of each partner for an improvement of the takeoff performance of the KH3Y configuration by redesign of the flap. It was targeted to perform a multipoint design for the takeoff configuration. Two main objectives are present:

1) Reduce drag for an improved climb performance.

2) Maintain or increase lift coefficients for lower takeoff speeds and therefore reduced takeoff field length.

A. Optimization Case Definition

The baseline of the design study is the DV06 wing section of the KH3Y model, now in takeoff configuration (TC216), as measured in the ETW in the EUROLIFT I project (Fig. 5). The coordinates have been provided, both in streamwise coordinates and with leading-edge sweep normalization applied [18]. The reference setting is the fixed second takeoff (TO2) setting with the flap deflected 22 deg and the slat deflected 20 deg. The DV06 wing section was chosen because it is in the middle of the outer wing part and between the slat and flap brackets, and so 2-D assumptions are most likely to be applied.

Because of the difficulties encountered at the mandatory test case optimizations, the description of the optimization problem for the flap design was specified much more carefully and with respect to the behavior of the 3-D model wing examined in the previous wind-tunnel experiments.

The design range is limited by two design points, depicted in Fig. 6, the first at $1.13V_S$ of the takeoff 22/20 (TO2) setting, which is the minimum allowable speed. The second design point is at $1.13V_S$ of the takeoff 16/8 (first takeoff, TO1) setting, which is the minimum speed for this setting, and therefore the speed where the setting will

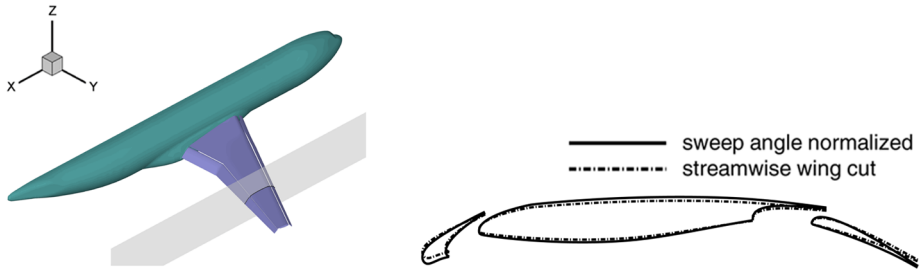

Fig. 5 Wing section of the KH3Y model in takeoff configuration (TO2) at the location of pressure row DV06 in streamwise and normalized coordinates.

be changed from the TO2 setting to the TO1 setting. These two design points cover the complete flight range according to Federal Aviation Administration airworthiness regulations [19].

To obtain comparable results, the flow conditions for the 2-D calculations have been adjusted to match the pressure distributions of the initial configuration. An analysis made by DLR gives corresponding 2-D flow for the flow conditions listed in Table 2, applying standard 2-D normalization of the on-flow conditions. The correctness of this procedure is indicated by the match of the pressure distributions shown in Fig. 7. These pressure distributions were also used by the partners to adjust their flow calculation procedures to obtain comparable initial conditions for the optimization.

Another focus was set on an approximation method that should allow for a reliable prediction of the 3-D wing behavior based on 2-D or 2.5-D (infinite swept wing) calculations. This was evident because the flap design obtained with the 2-D/2.5-D methods should be verified by the wind-tunnel test with the 3-D wing. The method chosen incorporates the assumption that the shape of the spanwise lift and drag distribution of the 3-D wing is unchanged due to the modifications of the flap, and can be scaled based on the lift and drag improvements of the 2-D wing section. This assumption is allowed for the investigated type of high-lift wing incorporating full-span slat and flap. Comparison of the previously calculated 2-D section data for the initial configuration and experimental data led to the relations

$$C_{L_{3\text{-D}}} = \gamma_{C_L} \times C_{L_{2.5\text{-D}}}, \qquad \gamma_{C_L} = 0.84173 \tag{2}$$

and

$$C_{D_{3\text{-D}}} = \gamma_{C_D}\left(C_{D_{2.5\text{-D}}} + \frac{C^2_{L_{2.5\text{-D}}}}{\pi\tilde{\Lambda}}\right), \qquad \tilde{\Lambda} = \Lambda \cdot \frac{\gamma_{C_D}}{\gamma^2_{C_L}} = 14.3926 \tag{3}$$

The definition of the objective function is based on the climb index

$$\begin{aligned} F_{\text{obj}}(\mathbf{x}) &= \sum_{i=1,2} w_i \cdot F_i(\mathbf{x}) \\ F_1(\mathbf{x}) &= -C^3_{L_{3\text{-D}}}/C^2_{D_{3\text{-D}}}|_{\alpha=8.00\,\text{deg}} \\ F_2(\mathbf{x}) &= -C^3_{L_{3\text{-D}}}/C^2_{D_{3\text{-D}}}|_{\alpha=11.91\,\text{deg}} \end{aligned} \tag{4}$$

at the limits of the design range with equal weighting factors $w_1 = w_2 = 0.5$. This performance indicator is better suited for high-lift performance improvement than the lift-to-drag ratio, because it has an additional weighting on the lift coefficient. The climb index itself is derived from the climb speed, which is approximately

$$\frac{w}{V} \approx \frac{T}{G} - \frac{C_D}{C_L} \Rightarrow w \approx \frac{1}{\sqrt{C_L}}\frac{T}{G} - \frac{C_D}{C_L^{3/2}} \tag{5}$$

Constraints have to be applied to prevent loss of lift coefficient and increase of nose down pitching moment. An additional penalty

$$P(\mathbf{x}) = \begin{cases} 0 & \forall\ \Delta x_F \le 0 \\ |F_{\text{obj}}(\mathbf{x}_{\text{ini}})| \cdot (200 \cdot \Delta x_F^2) & \forall\ \Delta x_F > 0 \end{cases} \tag{6}$$

is added to take into account weight increase of the kinematics system with larger flap deployment and was specified on industrial request.

The degrees of freedom for the design are the 3 degrees of freedom for the flap deflection and the part of the flap shape that is hidden when the flap is retracted. For further identification, this test case is named TC302.

Table 2 Correlation of flow conditions for comparable flow between 3-D experiment and 2-D/2.5-D calculation

		3-D	2.5-D	2-D (norm.)
Design point 1 (upper limit)	M	0.2	0.2	0.17146
	Re	15×10^6	15×10^6	11.03×10^6
	α	8.00	8.25	9.599
	C_L	1.69235	2.01694	2.74425
Design point 2 (lower limit)	M	0.2	0.2	0.17146
	Re	15×10^6	15×10^6	11.03×10^6
	α	11.91	12.75	14.785
	C_L	2.05364	2.40691	3.27484

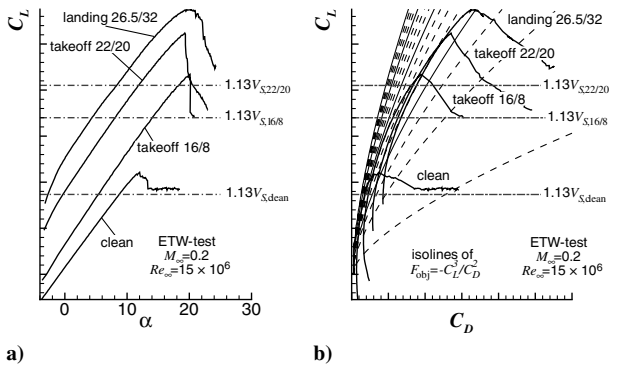

Fig. 6 Limits of the design range for KH3Y configuration TO2 (22/20) derived from wind-tunnel data: a) lift vs angle of attack of the reference aircraft configuration for different settings; b) lift vs drag of the reference aircraft configuration for different settings together with the isolines (dashed) of the objective function (minimum flight speed for each setting marked with dash-dotted line).

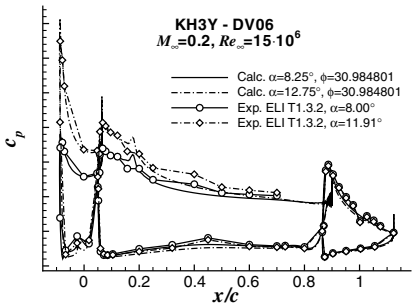

Fig. 7 Comparison of experimentally determined pressure distributions at DV06 for two angles of attack and 2-D flow calculations by DLR.

Table 3 Classification of the methods applied by the partners for the flap design

Partner	Solver type	Grid type	Dimension	Optimization algorithm
AD	Panel-BL		3-D	Best engineering practice
CIRA	Euler-BL	Structured	2-D	Genetic algorithm
DLR	RANS	Structured	2-D	Simplex algorithm Differential evolutionary algorithm
FOI	RANS	Unstructured	2.5-D	Quasi-Newton method
ONERA	RANS	Structured chimera	2-D 2.5-D	Conjugate gradient

B. Applied Methods

Table 3 briefly summarizes the methods used by the involved partners for the design of the flap. A more complete description of the details of the methods applied on this design case has been published during the EUROGEN 05 conference [20–23]. Compared to the mandatory test case described earlier, additional methods were also used to investigate dependencies of the optimum solution on the calculation method.

DLR made some preliminary tests on this design case applying gradient-based, gradient-free, as well as stochastic methods [21]. The final design was obtained using a differential evolutionary algorithm (DE) [24]. DE has been tested both on benchmark problems [25] and on real problems [26], and it often appears to be the best performing algorithm for finding the global optimum.

ONERA assessed the influence of 2-D and 2.5-D flow calculations by performing optimizations for the normalized wing section and for the infinite swept wing. As indicated by the mandatory test case, CIRA assessed the usability of the Euler-BL method for this design case in advance of the optimization. Because the differences of the RANS and the Euler-BL results for the baseline flap had been very small, it was again decided to use the Euler-BL approach for this design.

Airbus Germany's part of the work was to apply their best engineering tools instead of performing numerical optimization for this design. This would allow direct demonstration of the benefits of the numerical optimization approach compared with today's engineering work methods. The method AD applied incorporates the 2-D panel-boundary-layer method that is coupled to a 3-D lifting line method.

C. Optimization Results

All partners distributed their optimization results including the following: 1) aerodynamic coefficients, surface pressure distributions, and flowfields of the initial and optimized configuration; 2) history of optimization in terms of design variables, aerodynamic coefficients, single objectives, and global objective; and 3) optimization statistics in terms of number of needed CFD calculations, CPU time, and turnaround (wall clock) time.

A work share has been agreed by the partners to achieve as much information on the design case as possible. It was planned that some partners (ONERA, CIRA) should focus on setting optimization, and others (DLR, FOI) should investigate flap shape and setting optimization. Because of unsatisfactory results of the setting optimization, CIRA decided to also perform a flap shape and setting optimization. Table 4 summarizes the available data. The obtained optimum solutions are depicted in Fig. 8. Table 5 lists the objective function improvements predicted by the numerical optimization method. It has to be pointed out that these values are derived from the method used within the optimization cycle and may not be directly comparable.

1. *Flap Setting Design*

First setting optimizations carried out by ONERA predicted a much larger improvement (values in parentheses of Table 5) than all the shape and setting designs. This indicated a large dependency of the improvements on the flow solving procedure. New results obtained by ONERA with adapted numerical setups lead to an improvement lower than when considering both shape and setting and are comparable to CIRA's result. The difference between 2-D and 2.5-D calculation method is of minor importance. This verifies, to some extent, that the 2-D methodology is appropriate for this kind of design. The CIRA setting design shows less improvements and a different direction of setting changes. Whereas the movement for the ONERA design is in the direction to close the gap, the CIRA design moves the flap downstream while retaining the flap gap. In both cases, the flap angle is unchanged.

2. *Flap Shape and Setting Design*

The combined shape and setting design shows an even larger variety of obtained solutions to the design problem. This is somewhat expected, because the additional parameters increase the design space and the chance of multiple locally optimal configurations. The spreading of the predicted improvements in contrast is much smaller than for the pure setting design mentioned earlier. An interesting side effect for the shape and setting design is observed when virtually connecting the leading edges of all three designs (dashed line in Fig. 8). It is seen that the leading edges are almost aligned in a specific direction, indicating an optimum correlation of gap and overlap when changing the shape.

3. *Best Engineering Practice*

The major conclusion from best engineering practice design is a failure of improving the performance while taking into account the constraints. An improvement of the takeoff performance was only achievable when violating either the lift or pitching moment constraints. This result is not as astonishing, because the baseline was formerly designed using these methods.

Table 4 Summary of performed optimization calculations

Partner	Design variables	Dimension	Optimization algorithm
AD	Shape and setting	3-D	Best engineering practice
CIRA	Setting Shape and setting	2-D	Genetic algorithm
DLR	Shape and setting	2-D	Simplex algorithm Differential evolutionary algorithm Variable metric method
FOI	Shape and setting	2.5-D	Quasi-Newton method
ONERA	Setting	2-D 2.5-D	Conjugate gradient

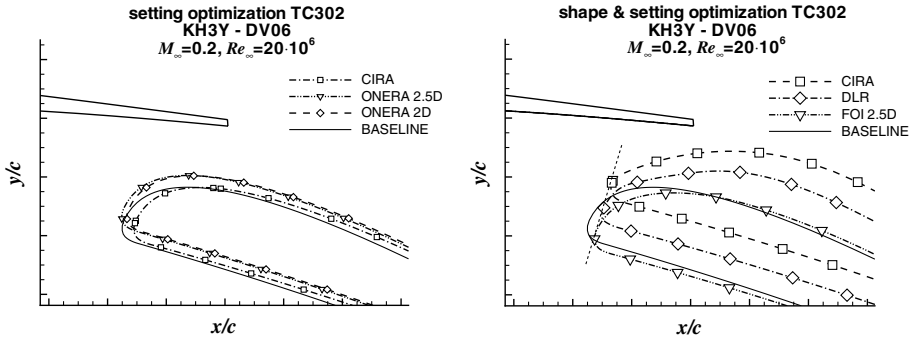

Fig. 8 Designed flap settings and shapes resulting from numerical optimization.

D. Cross Checking of Optimization Results and Selection for Wind-Tunnel Entry

As seen from the results, it is necessary to compare the different design optimization results with the same flow solving procedure to be able to judge the best obtained results. For this reason, the cross calculation of the results was implemented in the work program. Within these cross calculations, different partners calculate the design optimization results from other partners. By this, a set of results are achieved that allows eliminating the dependencies of the result on the solving procedure. This is a prerequisite to be able to select the best obtained design for wind-tunnel testing.

A common request for these calculations was to use the highest level of simulation accuracy. For this reason, CIRA recomputed all configurations using their RANS solver instead of the Euler-BL solver applied for the optimization. DLR delivered their results computed on the finest mesh level instead of the second multigrid level as used in the design.

Figure 9 shows the tendencies reported by the different partners for the different "optimal" solutions, which were the foundation for the selection of the configuration to test. There are some differences observed compared with the values reported in Table 5. The values for CIRA's calculation of their own designs differ due to the change to RANS calculations for the cross calculations. The improvements predicted by the Euler-BL calculation method are not fully retained when calculated using RANS. The FOI values differ slightly due to the use of grids with a higher spatial resolution for the cross calculations. The benefit of the ONERA designs have not been verified by other partners' calculations.

It is seen that the tendencies are very similar, independent from the partner's method applied. It shows that the DLR design is predicted to have the highest potential for improvement. For this reason, the DLR shape has been selected for application to the wind-tunnel model.

Another fact, not shown in the figure, is that the prediction of the pure aerodynamic performance of the CIRA design without the geometrical penalty gives similar improvements as the DLR design, although the setting of the flap is quite different. To investigate this in more detail, additional calculations have been performed for the comparison of DLR and CIRA flap shape design. For this investigation, the flap of the one design has been positioned at the setting of the other one. As an example, Fig. 10 shows performance

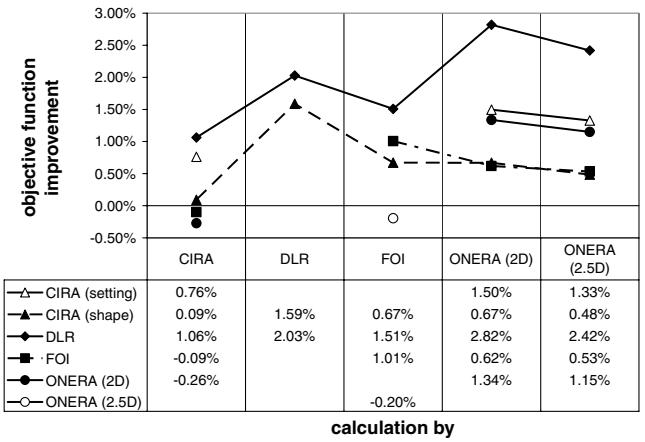

Fig. 9 Comparison of improvements resulting of cross calculations of the different partners.

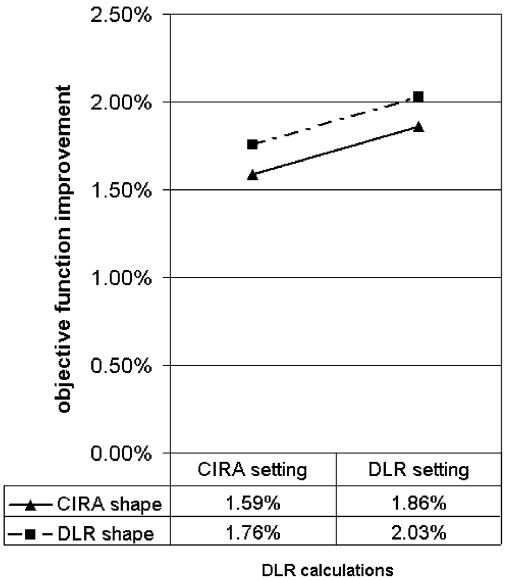

Fig. 10 Breakdown of improvements of CIRA and DLR designs on shape and setting effects based on DLR calculations.

Table 5 Summary of obtained takeoff performance improvements predicted by optimization methods

Partner	Design variables	Dimension	Objective improvement
CIRA	Setting	2-D	$\Delta F_{obj} = 1.44\%$
	Shape and setting		$\Delta F_{obj} = 2.54\%$
ONERA	Setting	2-D	$\Delta F_{obj} = 1.69\%$ (8.17%)[a]
		2.5-D	$\Delta F_{obj} = 1.22\%$ (7.49%)[a]
DLR	Shape and setting	2-D	$\Delta F_{obj} = 1.97\%$
FOI	Shape and setting	2.5-D	$\Delta F_{obj} = 0.9\%$
AD	Best practice	3-D	$\Delta F_{obj} = 0\%$

[a]Initial values (see Sec. III.C).

improvements without the geometric penalty according to DLR calculations for the two shapes at the two settings. There is only a slight advantage for the DLR flap shape predicted. This result is underlined when comparing the shape and the pressure distribution for the same setting, as depicted in Fig. 11. The difference between both shapes is visible only in a small part of the flap suction peak. This comparison shows that both flap shapes are equivalent, and the differences might have their major reason in the differences of the flap shape parameterization applied by the partners for this study.

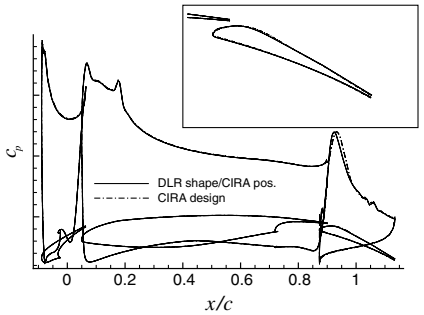

Fig. 11 Comparison of CIRA and DLR flap shape designs at the same setting and comparison of corresponding pressure distributions.

This result raises the question if the small dependence of the aerodynamic behavior on the large variation of the flap setting is artificial to the computations or if it can be proven experimentally. For this reason, it was finally decided not to investigate the optimum setting for the baseline flap shape in the wind-tunnel test. Instead, it was decided to test the new flap with the flap shape designed by DLR at the two settings resulting from DLR and CIRA flap shape and setting design.

IV. European Transonic Wind-Tunnel Verification

To verify the design optimization results obtained from numerical simulations, a wind-tunnel test has been conducted. To be as close as possible to future industrial needs, the optimization has been performed for high Reynolds numbers. For this reason, for the wind-tunnel test, an entry in the European transonic wind-tunnel facility had been planned from the beginning. The test for the verification of the design optimization work of this task was performed in May 2006.

A. Wind-Tunnel Model Setup

At first, the selected flap shape design has been applied to the KH3Y wind-tunnel model. Because the design investigations have all been for one 2-D wing section only, first, this shape has to be transferred to the 3-D flap of the model. This work has been done using the CAD software CATIA (V4). The software offers a wide range of lofting functions, ideally usable for this issue. For this lofting, the original flap shape has been divided on the upper and lower part to limit the modifications of the shape to the allowed range. Afterward, the designed flap shape has been transformed to other wing sections (kink, root, and tip) by scaling the length to the local flap chord and the thickness related to the local section thickness by affine transformation rules. Figure 12 shows a comparison of the original and newly designed 3-D model flap. The flap profile shape line at the upper flap in the figure shows the designed flap section. By the design method, it has been guaranteed that the flap shape is exactly met for the design section and the characteristics of the shape are maintained along the whole flap span. The position of the new flap for both settings has been transferred to the 3-D model related to the local flap chord, resulting in the most uniform setting distribution. By doing this, the characteristics of the setting are also maintained for the whole wing. Figure 13 shows the realized distribution of the setting values gap and overlap along the wingspan of the KH3Y model, which have been measured with a six-component coordinate measurement equipment. For measurement purposes, the new flap was equipped with pressure tab rows in four wing sections, including the design wing section DV06.

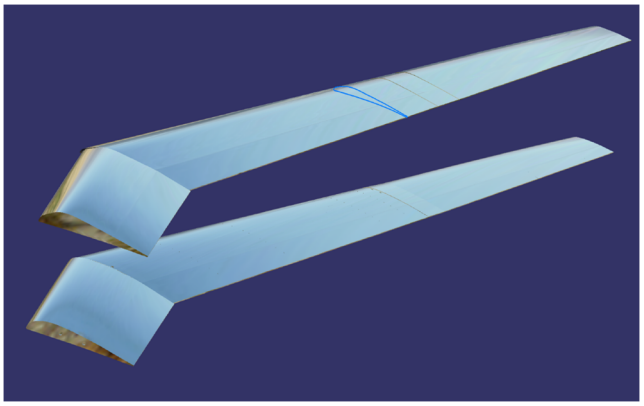

Fig. 12 Comparison of original 3-D model flap (lower) and newly designed model flap (upper); flap section profile in upper flap indicates design section.

B. Wind-Tunnel Test Program

Measurements have been conducted in ETW for all three configurations (denoted as baseline, DLRopt, and CIRAset) at three

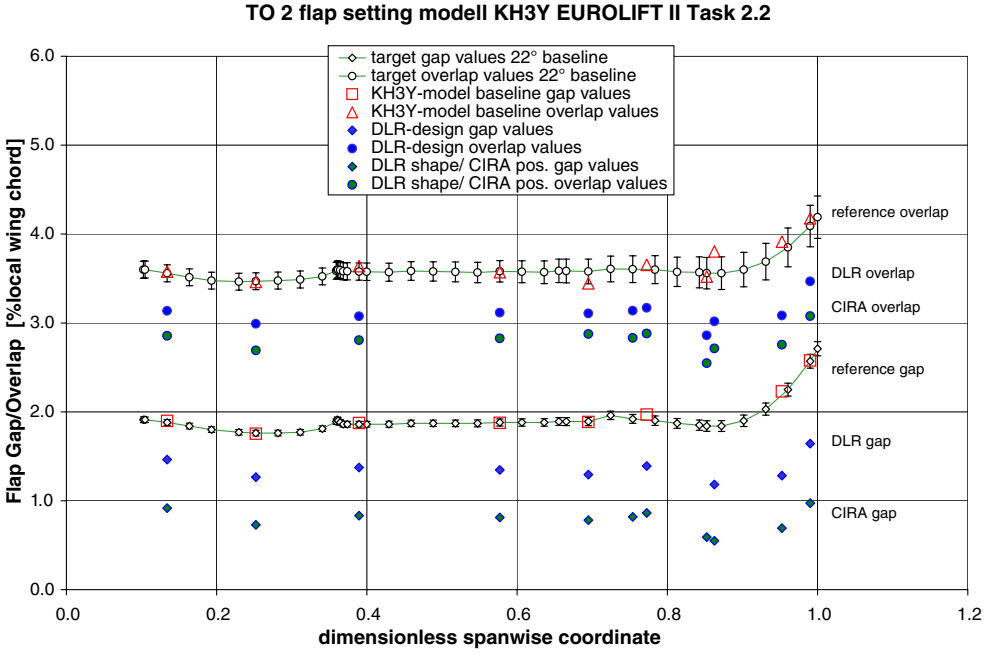

Fig. 13 Setting distribution along wingspan of the KH3Y model compared for the original flap and the newly designed flap at both setting positions, evaluated with six-component coordinate measurement equipment.

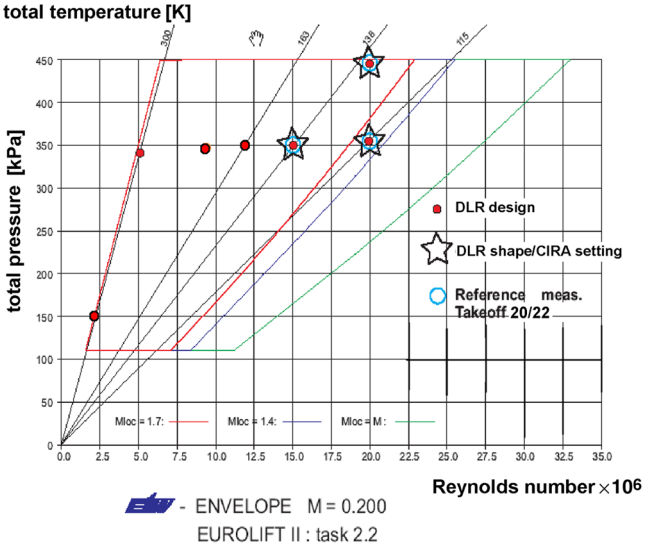

Fig. 14 Flow conditions investigated during the ETW entry for verification of the flap design.

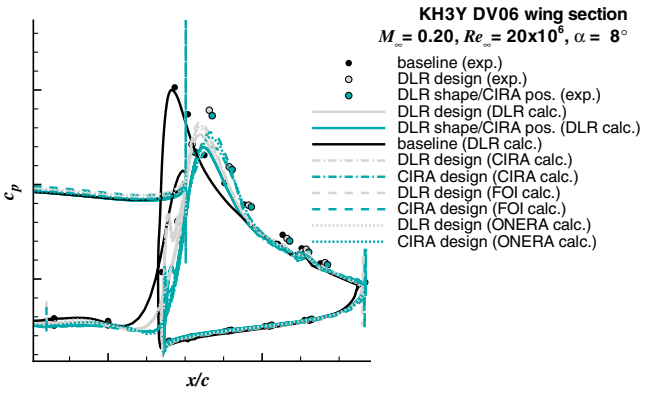

Fig. 16 Comparison of numerically predicted and experimentally measured pressure distributions on the flap for the newly designed flap in both investigated setting positions at the first design point for the design wing section DV06 (gray scale denotes configuration, line style indicates calculating partner).

wind-tunnel conditions (Fig. 14). The three major tunnel conditions cover two different Reynolds numbers: 1) $Re_\infty = 15 \times 10^6$, to be able to compare to former EUROLIFT I data, and 2) $Re_\infty = 20 \times 10^6$, corresponding to the design case description. The Reynolds number variation from 15 to 20 million has been obtained by a variation of stagnation temperature ($T_t = 138$ K and $T_t = 115$ K at $p_t = 3.5$ bar) and pressure ($p_t = 3.5$ bar and $p_t = 4.5$ bar at $T_t = 138$ K) independently. With this test program, it is possible afterward to distinguish clearly between Reynolds number effects and the influence of model deformations due to the pressurized tunnel. The DLRopt has been tested at additional points during the warm-up of the tunnel to ambient conditions at the end of the wind-tunnel test entry. All measurements have been preformed at the same Mach number $M_\infty = 0.2$.

C. Assessment of Optimization Results with Wind-Tunnel Data

Out of the large amount of data within this report, there is a focus on a comparison of the wind-tunnel data of the ETW entry and the CFD prediction during the numerical design work. First, the achieved improvement of the new flap design has been analyzed.

Figure 15 shows the relative improvement of the aerodynamic part of the optimization objective, neglecting the constraints, compared with the scaled CFD predictions resulting from the cross calculations (including ONERA's refined solution procedure). All the computationally predicted improvements generally show a very good agreement with the values obtained experimentally for the 3-D half-model. Also, the slope between the two design points is captured pretty well. Nevertheless, there are slight differences in the prediction between the two settings for the newly designed flap, depending on the partners' computational methods. On the other side, these differences are of similar order of magnitude as the scatter within the wind-tunnel data. Remembering that the cross computations have been performed for the original CIRA flap shape design, except for one DLR calculation, this also verifies the equivalence of the CIRA and DLR flap shapes.

In Fig. 16, an exemplary comparison of the pressure distributions on the flap is shown at the first design point $\alpha = 8$ deg for the design wing section DV06. For the baseline, only the DLR computation is plotted for comparison. The computations labeled CIRA design have been performed also on the CIRA shape, in contrast to the measurements made with the DLR shape. The comparison shows the spreading of the predictions of the flap flow and the flap suction peak is slightly underpredicted. Nevertheless, the change in the characteristics of the flap pressure distribution is well captured.

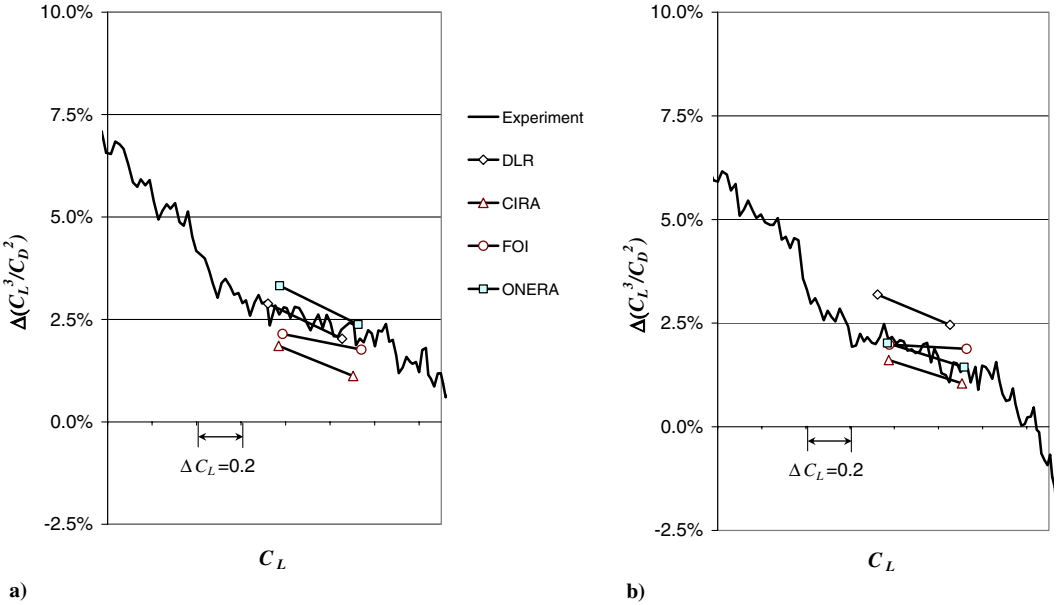

Fig. 15 Comparison of predicted relative improvement of aerodynamic performance compared with wind-tunnel data: a) DLR design, and b) CIRA design (computations) vs DLR flap at CIRA setting (experiment).

Also, the response of the wing pressure distribution on the change of flap shape and position agrees very well between computations and measurements. This verifies that the improvements observed in the wind tunnel are due to the flap shape and setting design and not from artificial side effects from somewhere else at the 3-D wing.

V. Conclusions

The objective of the EUROLIFT II flap design was the demonstration of the applicability of design methods based on computational fluid dynamics and numerical optimization methods for the design of high-lift systems for transport aircraft. A first study on a mandatory 2-D design case showed the readiness of the methods, as well as some limitations of the range of design issues to be addressed.

Based on this experience, a design study for takeoff performance improvement for the wing of the KH3Y model was performed, based on 2-D and 2.5-D wing section design. Special care has been taken for the setup of the calculations to be comparable to behavior of the 3-D wing. A detailed transformation method has been derived for this purpose to approximate the improvements of the 3-D wing based on the 2-D/2.5-D CFD predictions. The results obtained later by the wind-tunnel experiments approved the validity of this approach for the performance prediction of the investigated type of high-lift system with full-span slats and flaps.

The design has been performed at one wing section of the designated KH3Y model at two design points and a high Reynolds number related to real aircraft flight conditions. To make the best selection for wind-tunnel verification, all results of the numerical design optimizations of the different partners have been cross computed to eliminate dependencies of the result on the numerical setup of the design method. This additionally led, in one case, to an improved numerical setup for design optimization calculations.

The final selected design has been carefully transferred to the 3-D model flap using modern CAD systems. Special care has been taken to maintain the flap shape and setting characteristics of the design wing section along the whole wingspan. Resulting from the cross calculations, the new flap shape has been investigated at two different settings, which had been predicted to gain similar improvements. Measurements have been performed in the European cryogenic transonic wind-tunnel facility at different Reynolds numbers, including the design Reynolds number, to additionally account for Reynolds number and model deformation effects.

The comparison of numerically predicted improvements with experimental data shows an astonishing agreement. Detailed insight into flow properties by means of pressure distributions shows that the numerical methods are able to capture the physics responsible for the performance improvement. This result suggests that numerical optimization based on CFD can benefit the design of aircraft high-lift devices.

Acknowledgments

The work reported here has been funded by the European Commission within the Sixth Framework Program under contract no. AST 2004 502896. The authors want to mention Ralf Mertins, Airbus Germany, who performed the activities related to Airbus's participation, but was not able to contribute to this paper as an author. Centro Italiano Ricerche Aerospaziali wishes to thank Mark Drela for allowing the use of his MSES code in its research work.

References

[1] Hansen, H., Thiede, P., Moens, F., Rudnik, R., and Quest, J., "Overview About the European High Lift Research Programme EUROLIFT," *42nd AIAA Aerospace Sciences Meeting and Exhibit*, AIAA Paper 2004-767, 2004.

[2] Gerhold, T., and Evans, J., "Efficient Computation of 3-D-Flows for Complex Configurations with the DLR–Tau Code Using Automatic Adaptation," *Notes on Numerical Fluid Mechanics*, edited by W. Nitsche, H.-J. Heinemann, and R. Hilbig, Vol. 72, Viewig, Brunswick, Germany, 1998, pp. 178–185.

[3] Drela, M., *A User's Guide to MSES 2.95*, MIT Computational Aerospace Sciences Lab., Cambridge, MA, Sept. 1996.

[4] Kroll, N., Rossow, C. C., Becker, K., and Thiele, F., "The MEGAFLOW project," *Aerospace Science and Technology*, Vol. 4, No. 4, 2000, pp. 223–237. doi:10.1016/S1270-9638(00)00131-0

[5] Brodersen, O., Hepperle, M., Ronzheimer, A., Rossow, C.-C., and Schöning, B., "The Parametric Grid Generation System MegaCads," *5th International Conference on Numerical Grid Generation in Computational Field Simulation*, edited by B. K. Soni, J. F. Thompson, J. Häuser, and P. Eisemann, National Science Foundation, Arlington, VA, 1996, pp. 353–362.

[6] Eliasson, P., "EDGE, A Navier–Stokes Solver for Unstructured Grids," Swedish Defence Research Agency FOI-R-0298-SE, Stockholm, Nov. 2001.

[7] Amoignon, O., Pralits, J. O., Hanifi, A., Berggren, M., and Henningson, D. S., "Shape Optimization for Delay of Laminar-Turbulent Transition," *AIAA Journal*, Vol. 44, No. 5, 2006, pp. 1009–1024. doi:10.2514/1.12431

[8] Gazaix, M., Jolles, A., and Lazareff, M., "The elsA Object-Oriented Computational Tool for Industrial Applications," *23rd Congress of ICAS*, International Council of the Aeronautical Sciences 2002-1.10.3.1, Sept. 2002.

[9] Wilcox, D., "Simulation of Transition with a Two-Equation Turbulence Model," *25th AIAA Fluid Dynamics Conference*, AIAA Paper 94-2386, June 1994.

[10] Goncalves, E., and Houdeville, R., "Reassessment of the Wall Function Approach for RANS Computations," *Aerospace Science and Technology*, Vol. 5, No. 1, 2001, pp. 1–14. doi:10.1016/S1270-9638(00)01083-X

[11] Eliasson, P., "CFD Improvements for High-Lift Flows in the European Project EUROLIFT," *21st AIAA Applied Aerodynamics Conference*, AIAA Paper 03-3795, June 2003.

[12] Vicini, A., and Quagliarella, D., "Inverse and Direct Airfoil Design Using a Multiobjective Genetic Algorithm," *AIAA Journal*, Vol. 35, No. 9, 1997, pp. 1499–1505. doi:10.2514/2.274

[13] Vicini, A., and Quagliarella, D., "Airfoil and Wing Design Through Hybrid Optimization Strategies," *AIAA Journal*, Vol. 37, No. 5, 1999, pp. 634–641. doi:10.2514/2.764

[14] Frommann, O., *Synaps Pointer Pro V2.50*, Synaps Ingenieur-Gesellschaft mbH, Bremen, Germany, 2002.

[15] Rowan, T., "Functional Stability Analysis of Numerical Algorithms," Ph.D. Thesis, Dept. of Computer Sciences, Univ. of Texas, Austin, TX, 1990.

[16] Nocedal, J., and Wright, S., *Numerical Optimization*, Springer Series in Operations Research, Springer, New York, 1999.

[17] Vanderplaats, G. N., "CONMIN: for Constrained Function Minimization," NASA TMX 62282, 1973.

[18] Wild, J., Mertins, R., Quagliarella, D., Brezillon, J., Germain, E., Amoignon, O., and Moens, F., "Realistic High-Lift Design of Transport Aircraft by Applying Numerical Optimization," *ECCOMAS CFD 2006 Conference* [CD-ROM], European Community on Computational Methods in Applied Sciences Paper No. 191, 2006.

[19] Federal Aviation Administration, "Airworthiness Standards: Transport Category Airplanes," Federal Aviation Regulations, Pt. 25, 2006.

[20] Amoignon, O., Pralits, J. O., Hanifi, A., Berggren, M., and Henningson, D. S., "Toward Optimal Flap Design for Takeoff Performance," *Proceedings of Evolutionary and Deterministic Methods for Design, Optimization, and Control with Applications to Industrial and Societal Problems EUROGEN 2005*, edited by R. Schilling, W. Haase, J. Périaux, H. Baier, and G. Bugeda, Technische Universität München, Fakultät für Maschinenwesen, Lehrstuhl für Fluidmechanik [CD-ROM], ISBN: 3-00-017534-2, 2005.

[21] Brezillon, J., and Wild, J., "Evaluation of Different Optimisation Strategies for the Design of a High-Lift Flap Device," *Proceedings of Evolutionary and Deterministic Methods for Design, Optimization, and Control with Applications to Industrial and Societal Problems EUROGEN 2005*, edited by R. Schilling, W. Haase, J. Périaux, H. Baier, and G. Bugeda, Technische Universität München, Fakultät für Maschinenwesen, Lehrstuhl für Fluidmechanik [CD-ROM], ISBN: 3-00-017534-2, 2005.

[22] Moens, F., "Numerical Optimisation of the Flap Position of a Three-Element High-Lift Airfoil in 2-D and 2.5-D Flow Using Navier–Stokes Solver, ONERA," *Proceedings of Evolutionary and Deterministic Methods for Design, Optimization, and Control with Applications to Industrial and Societal Problems EUROGEN 2005*, edited by R. Schilling, W. Haase, J. Périaux, H. Baier, and G. Bugeda, Technische Universität München, Fakultät für Maschinenwesen, Lehrstuhl für Fluidmechanik [CD-ROM], ISBN: 3-00-017534-2, 2005.

[23] Quagliarella, D., and Vitagliano, P. L., "Evolutionary Optimization of the EUROLIFT II Takeoff Design Case," *Proceedings of Evolutionary and Deterministic Methods for Design, Optimization, and Control with Applications to Industrial and Societal Problems EUROGEN 2005*, edited by R. Schilling, W. Haase, J. Périaux, H. Baier, and G. Bugeda, Technische Universität München, Fakultät für Maschinenwesen, Lehrstuhl für Fluidmechanik [CD-ROM], ISBN: 3-00-017534-2, 2005.

[24] Storn, R., and Price, K., "Differential Evolution: A Simple and Efficient Adaptive Scheme for Global Optimization over Continuous Spaces," International Computer Science Inst. TR-95-012, Berkley, CA, 1995.

[25] Vesterstrøm, J., and Thomsen, R., "A Comparative Study of Differential Evolution, Particle Swarm Optimization, and Evolutionary Algorithms on Numerical Benchmark Problems," *Proceedings of the 2004 Congress on Evolutionary Computation*, Vol. 2, Inst. of Electrical and Electronics Engineers, New York, 2004, pp. 1980–1987.

[26] Ursem, R. K., and Vadstrup, P., "Parameter Identification of Induction Motors Using Differential Evolution," *Proceedings of the Fifth Congress on Evolutionary Computation (CEC-2003)*, Inst. of Electrical and Electronics Engineers, New York, 2003, pp. 790–796.